



1 **Inter-Calibration of nine UV sensing instruments over**

2 **Antarctica and Greenland since 1980**

3

4 Clark Weaver^{1,2}, Pawan K. Bhartia¹, Dong L. Wu³, Gordon Labow^{1,4}, David Haffner^{1,4}

5 ¹ Atmospheric Chemistry and Dynamics Branch, NASA Goddard Space Flight Center,
6 Greenbelt, MD 20771, USA.

7

8 ² Earth System Science Interdisciplinary Center (ESSIC), University of Maryland
9 College Park, MD 20742, USA

10

11 ³ Climate and Radiation Laboratory, NASA Goddard Space Flight Center, Greenbelt, MD
12 20771, USA.

13

14 ⁴ Science Systems and Applications (SSAI), Inc., Lanham, MD 20706, USA.

15

16 *Correspondence to:* Clark Weaver clark.j.weaver@nasa.gov



1 **Abstract**

2 Nadir viewed intensities (radiances) from nine UV sensing satellite instruments are calibrated
3 over the East Antarctic Plateau and Greenland during summer. The calibrated radiances from
4 these UV instruments ultimately will provide a global long-term record of cloud trends and cloud
5 response from ENSO events since 1980. We first remove the strong solar zenith angle
6 dependence from the intensities using an empirical approach rather than a radiative transfer
7 model. Then small multiplicative adjustments are made to these solar zenith angle normalized
8 intensities in order to minimize differences when two or more instruments temporally overlap.
9 While the calibrated intensities show negligible long-term trend over Antarctica, and a
10 statistically insignificant UV albedo trend of -0.05 % per decade over the interior of Greenland,
11 there are small episodic reductions in intensities which are often seen by multiple instruments.
12 Three of these darkening events are explained by boreal forest fires using trajectory modeling
13 analysis. Other events are caused by surface melting or volcanoes. We estimate a 2-sigma
14 uncertainty of 0.35% for the calibrated radiances.

15

16 **1. Motivation**

17 In 1980 the Nimbus-7 spacecraft carried the first **Solar Backscatter in the UV (SBUV)**
18 instrument into low earth orbit to measure total column ozone. Since then, NOAA has
19 deployed a suit of SBUV-2 instruments on board the NOAA-9, 11, 14, 16, 17, 18 and 19
20 spacecrafts. Since they were all nadir viewing and thus had limited spatial coverage, NASA
21 also deployed a suite of mapping instruments: Nimbus-7 TOMS (1980), Earth Probe TOMS
22 and the Nadir Mapper (NM) instrument of the Suomi NPP Ozone Mapping Profiler Suite
23 (OMPS, 2012). True to their design, they have provided a long-term satellite data record of



1 ozone products; however, they also were intended to measure the earth's reflectivity in the
2 UV at wavelengths insensitive to ozone (331 and 340nm). Aside from a few publications
3 (Herman et al. (2013), Labow et al. (2011) and Weaver et al. (2015)), this data set has not
4 been fully exploited. Our ultimate goal is a long-term record of a UV cloud product that can
5 be directly compared with climate models. This paper details the first step: the inter-
6 calibration of radiances from the suite of nadir viewing instruments.

7 **2. Previous calibration of UV Satellite records**

8 The backbone of our data record is the suite of eight SBUV instruments starting with the
9 Nimbus-7 in 1980, and ending with NOAA-19 in 2013. Thereafter we use Nadir Mapper
10 (NM) instrument on the Suomi NPP OMPS. Each instrument provides narrowband
11 backscattered intensities near the 340 nm wavelength. We use a radiative transfer model
12 to account for the small differences in each instrument's center wavelength (see Appendix).
13 Regular sun-viewing irradiance measurements (F_{sun}) are made, typically weekly, to provide
14 long-term calibration information. The measured intensities are normalized by F_{sun} , and
15 multiplied by π . Throughout this study I refers to the sun normalized intensities.

16

17 We start with intensities that have already been calibrated to account for instrument
18 effects such as hysteresis (see Deland et al 2012), and that are reported in the Level-2
19 datasets for each instrument. The first seven SBUV/2 data sets were previously calibrated
20 by characterizing the instruments over the East Antarctic Plateau ice sheet using
21 **Lambertian Equivalent Reflectivity** (LER, Huang L.-K. et al. 2003 and Herman et al. 2013).



1 Using a radiative transfer model to calculate LER from the observed intensities removes
2 much of the solar zenith angle (θ_o) dependence, but not all; over the ice sheets LER still
3 decreases with θ_o especially at high θ_o . While they did an excellent job of characterizing
4 the first seven SBUV/2 instruments, two additional sensors need to be intercalibrated to
5 extend our record forward: the SBUV2 on NOAA-19, and the Suomi NPP OMPS. Rather than
6 calibrate these additional instruments with a radiative transfer model using LER, we use an
7 empirical approach to remove the solar zenith angle dependence on intensity. Using these
8 θ_o -normalized intensities, we inter-calibrate the UV sensors over the East Antarctic Plateau
9 and the Greenland ice sheets.

10 **3. Empirically based inter-calibration**

11 Satellite observed Nadir-viewed intensities over the Antarctic and Greenland ice sheets
12 have an almost linear relationship with solar zenith angle that is easily fitted with a 4-term
13 polynomial. Figure 1 shows the relationship over both ice sheets for all observations
14 sampled by the SBUV2 on NOAA-16. With a drifting orbit and long lifetime (2001-2014)
15 NOAA-16 sampled a wide range of solar zenith angles so we choose it as our reference
16 instrument. The polynomial fit uses all observations over the instrument's 15 year lifetime
17 and so provides a most probable intensity that the NOAA-16 SBUV2 would observe for a
18 given θ_o . Our calibration approach is to remove the solar zenith angle dependence from the
19 observed intensities (I_{obs}) by using the reference polynomial fits shown in Figure 1. We can
20 test if an observed intensity is high or low compared with the NOAA-16 SBUV2 reference
21 by calculating a fractional deviation in terms of intensity (δI) from Equation 1. For
22 example, the right panel of Figure 1 shows an anomalously low intensity sampled over a



1 dark scene ($I_{\text{obs}}^{\text{dark scene}}$) observed at a solar zenith angle ($\theta_{\text{o}}^{\text{dark scene}}$); it is compared with
2 the intensity that NOAA-16 would likely have observed at that solar zenith angle ($\xi(\theta_{\text{o}}^{\text{dark}}$
3 $\text{scene})$). The difference is divided by I_{obs} to produce a fractional deviation in intensity δI .

$$4 \quad \delta I = \frac{I_{\text{obs}} - \xi(\theta_{\text{o}})}{I_{\text{obs}}} \quad \text{Equation 1}$$

5 Each UV instrument has its own unique I_{obs} to θ_{o} relationship mainly because the
6 photomultiplier tube (PMT) for each instrument has a slightly different response function.
7 The underlying scene UV albedo (averaged over an instrument's lifetime) could be slightly
8 different for each instrument, which would also change the I_{obs} to θ_{o} relationship, but we
9 expect the Antarctic plateau albedo to be stable over time. The SBUV PMTs are designed to
10 have a zero-offset bias, i.e. zero current response when there are zero photon counts. Over
11 Antarctica the polynomial appears to have $I_{\text{obs}}=0$ at a solar zenith angle of 90° , consistent
12 with this instrument design (Figure 1). One needs to pay particular attention to make sure
13 the θ_{o} used is exactly simultaneous with the intensity, since the SBUV instruments have a
14 *different θ_{o} for each wavelength.*

15

16 We also show estimates of Intensity calculated by the radiative transfer model VLIDORT
17 (**V**ector **L**inearized **D**iscrete **O**rdinate **R**adiative **T**ransfer package, Spurr, 2006). Here we
18 assume Lambertian surface albedo of .95, and Rayleigh atmosphere with surface pressure
19 of 663 hPa. The number of half-space quadrature streams is 40; the number of stokes
20 vector parameters is 3. At first glance the VLIDORT simulation appears to simulate the



1 observations, but the slope of the simulation is slightly different than the observations
2 (right panel of Figure 1). We tried using the I to θ_0 relationship simulated by VLIDORT as a
3 reference (instead of using NOAA-16) but the δI was still too dependent on θ_0 which
4 complicated the analysis. Our method is similar but not as sophisticated as the sun-
5 normalized radiance validation approach described in Jaross et al (2008). They account for
6 the snow BRDF which we omit.

7

8 The suite of SBUV/2 instruments provides nadir observations with a 170x170km **Field Of**
9 **View (FOV)**. But the OMPS Mapper instrument has a smaller nominal 50x50km FOV, except
10 at the two most nadir viewing positions. Here the FOV widths are 20 and 30 km (Seftor et al
11 2017). For consistency, we only used the Mapper viewing positions that were within a
12 nadir-centered hypothetical 170x170km SBUV FOV and aggregated their intensities (area
13 weighted) prior to calculating δI . For each instrument we calculate the summertime annual
14 mean and plot the timeseries for both ice sheets (Figure 2).

15 **4. Adjusting the intensities**

16 The pre-calibrated intensities SBUV2 instruments on board NOAA-17, -18 and -19 appear
17 to be high biased and NOAA-14 low biased compared to our reference (Figure 2). As
18 described below, a cost-optimization approach is used to adjust the intensities and reduce
19 these disparities. Figure 2 only shows the summertime average δI , but when calibrating
20 instruments, it is instructive to examine the δI dependence on θ_0 for individual years. The
21 left panel of Figure 3a shows this for 2006 when the reference and three other instruments
22 were operational. The positive bias for NOAA-17 and 18 is consistent at all θ_0 bins. All



1 instruments show a similar skewed δI distribution, at each θ_o bin, toward low values of δI .
2 After adjustment, the biases are negligible (right panel Figure 3a).
3
4 To adjust intensities for a specific instrument a multiplicative factor (c_1) is chosen so that
5 the adjusted intensities are a linear function of the original intensities: $I_{adj} = c_1 * I_{original} + c_0$.
6 Adjusting the multiplicative factor (c_1) changes the gain, (intensity per observed photon
7 counts) of the instrument. To inter-calibrate all instruments with respect to NOAA-16 we
8 use a minimum-cost optimization algorithm to solve for a set of c_1 values that minimizes δI
9 disparities between temporally overlapping instruments. The c_1 for each instrument,
10 except the reference, is allowed to vary; Table 1 shows the gain changes made to each
11 instrument. Note that c_1 does not depend on time, so the interannual variability of a specific
12 SBUV instrument remains intact after the calibration.
13
14 Only the highest quality observations are used for the inter-calibration. Observations are
15 limited to θ_o less than 75° because at higher θ_o ozone absorption and straylight effects
16 become significant and contaminate results. Furthermore, SBUV observations that have a
17 grating drive error and observations that are likely impacted by PMT hysteresis are not
18 used to intercalibrate.
19
20 The grating drive selects the wavelength of a SBUV measurement. Sometimes, but not too
21 often, the grating drive selects the wrong value and the intensities are measured at a
22 wavelength different than the SBUV instrument's nominal wavelength. Inclusion of
23 observations with uncorrected grating errors will confuse our results, since our analysis



1 assumes that intensities to derive δI are all at the same wavelength. Fortunately, the
2 grating drive position is archived so we can apply a correction (see Appendix); however,
3 they are not used in the intercalibration, but are used in the later trend analysis. Figure 4
4 shows the summertime average empirically adjusted δI over both ice sheets after applying
5 the gain changes in Table 1. Solid circles exclude observations with grating drive errors and
6 open circles include corrected observations. There is clearly tighter match between
7 overlapping instruments compared with Figure 2. But there still are disparities between
8 overlapping instruments between 1997 and 1999 when multiple instruments suffer from
9 grating errors. It is disconcerting that our correction does not bring them in closer
10 alignment.

11

12 Both Nimbus-7 and to a lesser extent NOAA-9, suffered from PMT hysteresis. These earlier
13 PMTs were not able to quickly respond to the 4 orders of magnitude signal changes that
14 occur when the satellite first comes out of darkness on each orbit and the instrument sees
15 its first light. For Nimbus-7 hysteresis errors are between 4 and 9% at first light over
16 Antarctica and lessen as the PMT adjusts to the bright scenes over the ice sheet. By the time
17 the Nimbus-7 reaches Greenland the PMT is equilibrated and there is no hysteresis error.
18 (Maximum hysteresis errors of NOAA-9 are 2%). The intensity observations for these early
19 instruments have been corrected for hysteresis (Deland et al., 2001). Still, we initially were
20 unable to match Nimbus-7 with the other instruments; there was good agreement over
21 Antarctica but over Greenland Nimbus-7 was about 1% higher than the others (Figure 2).

22



1 Our remedy was to first calibrate the SBUV instruments *only* over Greenland where
2 Nimbus-7 is free of hysteresis error. As expected, all temporally overlapping instruments
3 agreed over Greenland, but over Antarctica Nimbus-7 was low by about 1% compared with
4 NOAA-9 and NOAA-11. Then we started removing Nimbus-7 observations; first those
5 within 1 minute of first light, then 2 minutes. With every minute of observations removed,
6 the disparity over Antarctica lessened. We achieved the good agreement seen in Figure 4
7 by removing 9 minutes of Nimbus-7 observations after first light.

8
9 Figure 5 shows the θ_0 dependence on the empirically adjusted δI for selected years. All the
10 SBUVs, except for Nimbus-7 and NOAA-9, have an almost flat (<0.005) δI dependence with
11 θ_0 . A flat θ_0 dependence indicates that the PMT response is similar to the NOAA-16. Over
12 Greenland δI dependence with θ_0 is not quite as flat (Figure 3b). The suppression of δI at
13 $\theta_0 > 57^\circ$ and time after first light < 9 minutes is seen for all years of Nimbus-7. Even though
14 these suppressed observations ($\theta_0 > 57^\circ$) were previously corrected for hysteresis,
15 artifacts remain and they are not used in any analysis.

16
17 Multiple instruments show coincident reduction of δI over Antarctica in January 1992
18 (Figure 4) most likely from aerosols transported to the Antarctic after the eruption of Mt
19 Pinatubo 6 months earlier in 1991 (left panel Figure 3c). The April 1982 eruption of El
20 Chichon likely contributed to the coincident reduction in 1983; other anomalies occur in
21 2001, 2010 and 2013. Likewise, there are coincident reductions in δI over Greenland.

22



1 To estimate the uncertainty in the SBUV intensity from instrument calibration alone we
2 first average the δI over the coincident satellites for each year; this merged time series is
3 the geophysical contribution. Absolute departures from this merged time series (Figure 6)
4 are attributed to instrument calibration uncertainty. Two times the standard deviation of
5 the fractional departures of all the SBUVs and OMPS (using both ice caps) is about 0.0035.
6 We conclude that annual averages of I have a 2-sigma uncertainty of 0.35%.

7

8 **5. Greenland Ice Sheet**

9 The albedo of the Greenland Ice Sheet is of interest because it contributes to changes in the
10 surface energy balance and surface melting. The variability of our UV δI record is
11 consistent with the MODIS albedo data set. A recent study presents time series of the
12 surface reflectance over the Greenland Ice Sheet from the Collection 5 (C5) and C6 MODIS
13 data sets (Casey et al. 2017). While the older C5 set shows strong darkening of the ice sheet
14 since 2000 (not shown), C6 has negligible trends that are not statistically significant. They
15 report surface reflectance for the channel closest to our UV channel (MODIS Band 3,
16 459nm) for dry snow conditions (locations with ice surface elevations > 2000 m) and for
17 wet snow conditions (elevations < 2000 m). For easier comparison we have transcribed the
18 data from their Figure 4 onto our Figure 4c. Many of the same episodic events in the MODIS
19 C6 record that limit measurements to wet snow conditions (solid blue trace Figure 4c) are
20 also seen by the UV instruments (Figure 4b and c): darkening in the NH summer of 2003,
21 2010 and 2012. The 2012 darkening was likely driven by anomalous surface melting over
22 Greenland. Satellite estimates of melt-day area from microwave brightness temperatures



1 (Nghiem et al., 2012) and mass loss from the NASA GRACE instrument both suggest strong
2 surface melting in 2012.
3
4 Surface or airborne light-absorbing aerosols that originate from boreal forest fires can
5 explain some of the other reductions of UV δI over Greenland. The 1995 darkening episode
6 is likely caused by forest fires in Canada. Using a trajectory model, Wotawa and Trainer
7 (2000) estimate that CO emitted from the large fires in western Canada reach Greenland on
8 1 July (their figure 2). Using a similar technique, Stohl et al 2006 estimate that CO from
9 Alaskan and Canadian fires in 2004 reached Summit Greenland on about 16 July. Their
10 figure 11 shows elevated levels of observed and trajectory-modeled CO from 16 July to 2
11 August. Finally, the global travels of smoke from the 2003 fires in South eastern Russia are
12 documented by Damoah et al. (2004) using a trajectory model and MODIS satellite images.
13 They estimate a 24 May arrival time over Greenland (their Figure 2). A time-series of daily
14 values of UV δI over Greenland show abrupt reductions by the SBUV instruments operating
15 on those dates (Figure 8). There are other dramatic darkening events, likely caused by
16 either forest fire smoke or surface melting (e.g. 2006 and 2008), that we could not find in
17 the literature.
18
19 While the shorter C6 record shows no apparent trend, our UV record shows a weak, though
20 statistically insignificant reduction in UV δI over Greenland: $-0.05 (0.06) \text{ decade}^{-1}$ at
21 locations with elevations > 2000 meters (Figure 4b). Impurities in the snow as detected by
22 insitu analysis are consistent with our observed trend. Polashenski (et al 2015) measured
23 the concentrations of light absorbing impurities (LAI) in 67 snow pits across North West



1 Greenland ice sheet in 2013 and 2014 and compared them with studies that analyzed snow
2 from the past 6 decades. Increases in black carbon or dust concentrations relative to recent
3 decades were small and corresponded to snow albedo reductions of at most 0.31, or ~0.05
4 per decade which is similar to our UV satellite estimate. The snow studies also record
5 episodic events that darken the snow 1-2%, similar to the 1995, 2003 and 2004 darkening
6 we see in the SBUV satellite record.

7

8 **6. Discussion / Summary**

9

10 The East Antarctic Plateau is the preferred ice sheet for performing radiance calibration. Its
11 very low temperatures and clear pristine conditions, except for the occasional volcanic
12 eruption, all maintain a stable surface albedo with time. In contrast, the interior Greenland
13 ice sheet is darkened every few years by air-borne particles from Boreal wild fires or from
14 albedo changes caused by widespread surface melting. Since we are not doing an absolute
15 calibration, but a relative calibration (using NOAA-16 as a reference instrument),
16 Greenland's albedo variations (~2%) test how well the SBUV instruments respond to
17 changes in the albedo. Moreover, including it in our calibration analysis enables a
18 characterization of instrument hysteresis errors mainly with Nimbus-7 over Antarctica.
19 Once removed, it matters little whether both ice sheets or only Antarctica are used to
20 determine the multiplicative gain coefficients (c_1), the UV δI trends over both ice sheets are
21 almost the same.

22



1 Intensities at the 340 nm wavelength channel observed by eight nadir-viewing SBUV
2 satellite instruments and the OMPS scanning instrument are intercalibrated over the
3 Antarctic and Greenland ice sheets. The approach is to compare observed intensities that
4 have been normalized by solar zenith angle. After the inter-calibration, we estimate a 2-
5 sigma uncertainty of 0.35% based on temporally overlapping sensors. Multiple instruments
6 respond in unison to known darkening events that sometimes can be explained by volcanic
7 aerosols, soot from boreal forest fires, or surface meltwater. These calibrated intensities
8 will be used to derive a UV cloud albedo record over the tropics and midlatitudes since
9 1980.

10

11 **Appendix - Accounting for small wavelength differences**

12 Each instrument provides narrowband backscattered intensities close to but not exactly at
13 340 nm wavelength. For example, the Nimbus-7, NOAA-9 and NOAA-14 have nominal
14 center wavelengths of 339.90, 339.75, 340.05 nm and Full Width Half Maximum (FWHM) of
15 1.0, 1.132 and 1.132nm, respectively. These seemingly small wavelength differences will
16 change observed intensities by several tenths of a percent at high solar zenith angles. Using
17 the VLIDORT Radiative Transfer Model we create a 2-dimensional table of intensities at 0.1
18 nm wavelength resolution and at 10° SZA resolution. A Lambertian surface of 0.95 albedo is
19 assumed. For each instrument we determine a simulated intensity I_{sim} by convolving the
20 instrument's FWHM across the center wavelength of the instrument. To account for the
21 wavelength and FWHM difference between a non-reference instrument (e.g. Nimbus-7)
22 and our reference instrument NOAA-16 we multiply the observed intensities from Nimbus-
23 7 by $I(\theta_o)_{sim}^{NOAA-16} / I(\theta_o)_{sim}^{Nimbus-7}$. Note that the wavelength correction is



1 dependent on solar zenith angle.

2

3

4 **References**

5

6 Damoah, R., N. Spichtinger, C. Forster, P. James, I. Mattis, U. Wandinger, S. Beirle, and A.
7 Stohl (2004), Around the world in 17 days— Hemispheric-scale transport of forest fire
8 smoke from Russia in May 2003, *Atmos. Chem. Phys.*, 4, 1311–1321.

9

10 DeLand, M.T., R.P. Cebula, L. Huang, S.L. Taylor, R.S. Stolarski, and R.D. McPeters, 2001:
11 Observations of “Hysteresis” in Backscattered Ultraviolet Ozone Data. *J. Atmos. Oceanic*
12 *Technol.*, 18, 914–924, [https://doi.org/10.1175/1520-](https://doi.org/10.1175/1520-0426(2001)018<0914:OOHIBU>2.0.CO;2)
13 [0426\(2001\)018<0914:OOHIBU>2.0.CO;2](https://doi.org/10.1175/1520-0426(2001)018<0914:OOHIBU>2.0.CO;2)

14

15 Deland, S. L. Taylor, L. K. Huang, and B. L. Fisher, 2012: Calibration of the SBUV version 8.6
16 ozone data product. *Atmos. Meas. Tech. Discuss.*, 5, 5151–5203, doi:10.5194/amt-d-5-5151-
17 2012.

18

19 Casey, K.A., C.M. Polashenski, J. Chen, and M. Tedesco, 2017: Impact of MODIS sensor
20 calibration updates on Greenland Ice Sheet surface reflectance and albedo trends. *The*
21 *Cryosphere*, 11, 1781-1795, doi:10.5194/tc-11-1781-2017.

22

23 Herman J. and Coauthors, 2013: A net decrease in the Earth’s cloud plus aerosol reflectivity
24 during the past 33 yr (1979–2011) and increased solar heating at the surface. *Atmos.*
25 *Chem. Phys.*, 13, 8505–8524, doi:10.5194/acp-13-8505-2013.

26

27 Huang, L.-K., R. P. Cebula, S. L. Taylor, M. T. DeLand, R. D. McPeters, and R. S. Stolarski, 2003:
28 Determination of NOAA-11 SBUV/2 radiance sensitivity drift based on measurements of
29 polar ice cap radiance. *Int. J. Remote Sens.*, 24, 305–314, doi:10.1080/01431160304978.

30

31 Jaross, G., and J. Warner, 2008: Use of Antarctica for validating reflected solar radiation
32 measured by satellite sensors. *J. Geophys. Res.*, 113, D16S34, doi:10.1029/2007JD008835.

33

34 Labow, G., Herman, J. R., Huang, L. K., Lloyd, S. A., DeLand, M. T., Qin, W., Mao, J., and
35 Larko, D. E.: Diurnal variation of 340 nm Lambertian equivalent reflectivity due to clouds and
36 aerosols over land and oceans, *J. Geophys. Res.*, 116, D11202, doi:10.1029/2010JD014980, 10,
37 2011.

38 McPeters, R. D., et al. (1996), *Nimbus-7 Total Ozone Mapping Spectrometer (TOMS) Data*
39 *Products User’s Guide*, NASA Ref. Publ., 1384, NASA Sci. and Tech. Inf. Branch, Washington,
40 D. C.

41 Nghiem, S. V., Hall, D. K., Mote, T. L., Tedesco, M., Albert, M. R., Keegan, K., et al. (2012).



- 1 The extreme melt across the Greenland Ice Sheet in 2012. *Geophysical Research Letters*, 39,
2 L20502. <http://dx.doi.org/10.1029/2012GL053611>.
- 3 Polashenski, C. M., J. E. Dibb, M. G. Flanner, J. Y. Chen, Z. R. Courville, A. M. Lai,
4 J. J. Schauer, M. M. Shafer, and M. Bergin (2015), Neither dust nor black carbon causing
5 apparent albedo decline in Greenland's dry snow zone: Implications for MODIS C5 surface
6 reflectance, *Geophys. Res. Lett.*, 42, 9319–9327, doi:10.1002/2015GL065912.
7
- 8 Seftor, C. J., G. Jaross, M. Kowitt, M. Haken, J. Li, and L. E. Flynn (2014), Postlaunch
9 performance of the Suomi National Polar-orbiting Partnership Ozone Mapping and Profiler
10 Suite (OMPS) nadir sensors, *J. Geophys. Res. Atmos.*, 119, 4413–4428,
11 doi:10.1002/2013JD020472.
12
- 13 Spurr, R. J. D., 2006: VLIDORT: A linearized pseudo-spherical vector discrete ordinate
14 radiative transfer code for forward model and retrieval studies in multilayer multiple
15 scattering media, *J. Quant. Spectrosc. Radiat. Transfer*, 102(2), 316–342,
16 doi:10.1016/j.jqsrt.2006.05.005
17
- 18 Stohl, A., et al. (2006), Pan-Arctic enhancements of light absorbing aerosol concentrations
19 due to North American boreal forest fires during summer 2004, *J. Geophys. Res.*, 111,
20 D22214, doi:10.1029/2006JD007216. Wiscombe, W. J., and S. G. Warren (1980), A model
21 for the spectral albedo of snow. I: Pure snow, *J. Atmos. Sci.*, 37(12), 2712–2733,
22 doi:10.1175/1520-0469(1980)037<2712:amftsa>2.0.co
23
- 24 Weaver, C., J. Herman, G. Labow, D. Larko, and L. Huang, 2015: Shortwave TOA Cloud
25 Radiative Forcing Derived from a Long-Term (1980–Present) Record of Satellite UV
26 Reflectivity and CERES Measurements. *J. Climate*, 28, 9473–9488,
27 <https://doi.org/10.1175/JCLI-D-14-00551.1>
28
- 29 Wotawa, G. and Trainer, M.: The influence of Canadian forest fires on pollutant
30 concentrations in the United States, *Science*, 288, 324–328, 2000.



1

Linear equation for empirical δI Adjustment

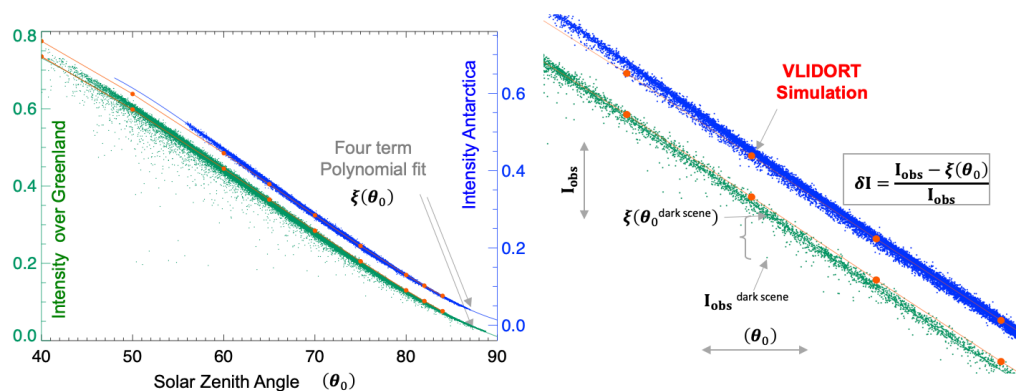
$$I_{\text{adj}} = c_1 * I_{\text{original}} + c_0$$

	c_0	c_1
Nimbus-7 SBUV	-	0.9913
NOAA-9 SBUV/2	-	1.0013
NOAA-11 SBUV/2	-	1.0002
NOAA-14 SBUV/2	-	1.0011
NOAA-16 SBUV/2	-	1.0000
NOAA-17 SBUV/2	-	0.9962
NOAA-18 SBUV/2	-	0.9936
NOAA-19 SBUV/2	-	0.9976
OMPS-Mapper		0.9972

2
3 Table 1. Gain c_1 and offset c_0 values used to make adjustments to observed intensities for
4 UV sensing instruments.



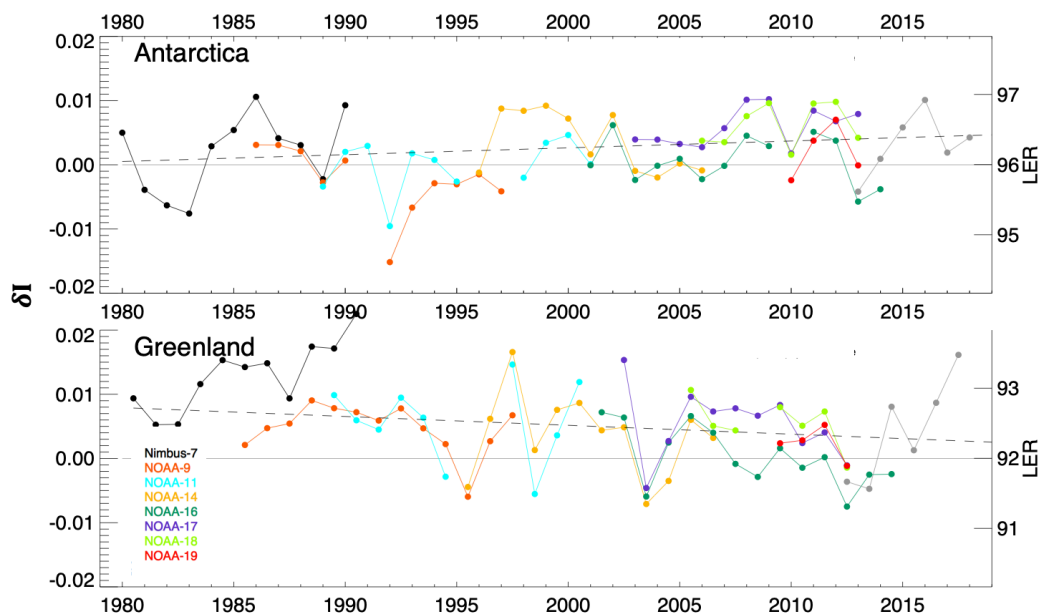
Figure 1



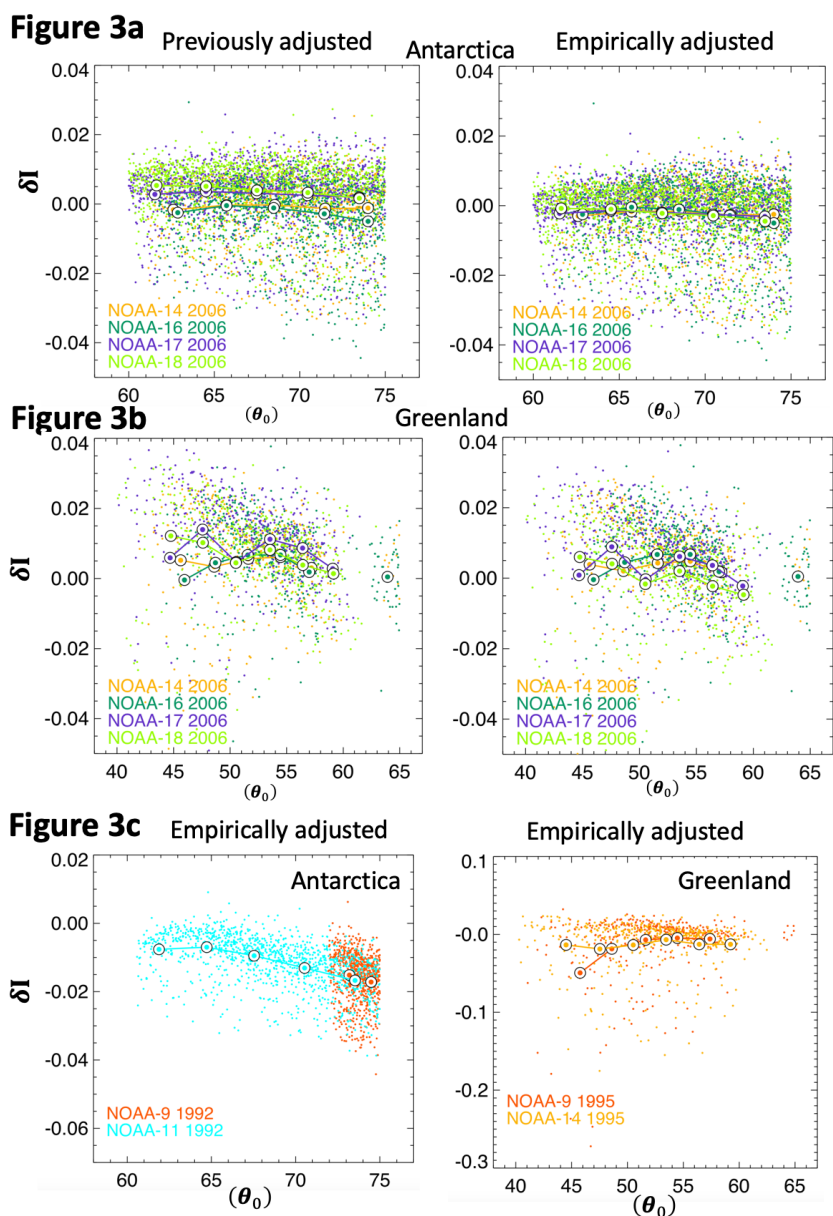
1
2 Figure 1. Figure A-1 Measured Intensity at 340 nm from the NOAA-16 SBUV versus Solar
3 Zenith Angle over the Antarctic Plateau (blue) and Greenland (green). Each point is a
4 nadir-viewed observation at the native Field of View (170 km by 170 km) during the
5 summer (fifteen days on either side of solstice). Also shown is a polynomial fit and a
6 radiative transfer simulation (red) assuming a Lambertian surface albedo of .95, a Rayleigh
7 atmosphere with surface pressure of 663 hPa. Note that the Greenland intensities are offset
8 from the Antarctic ones. The right panel shows a zoomed in view (see text for details).
9



Figure 2



- 1
- 2 Figure 2. Inter-annual variability of previously calibrated δI for the SBUV instruments
- 3 (colored) and OMPS mapper (grey) over Antarctica and Greenland. The right-hand axis
- 4 shows the corresponding change in LER.



1

2

3

4

5

6

7

8

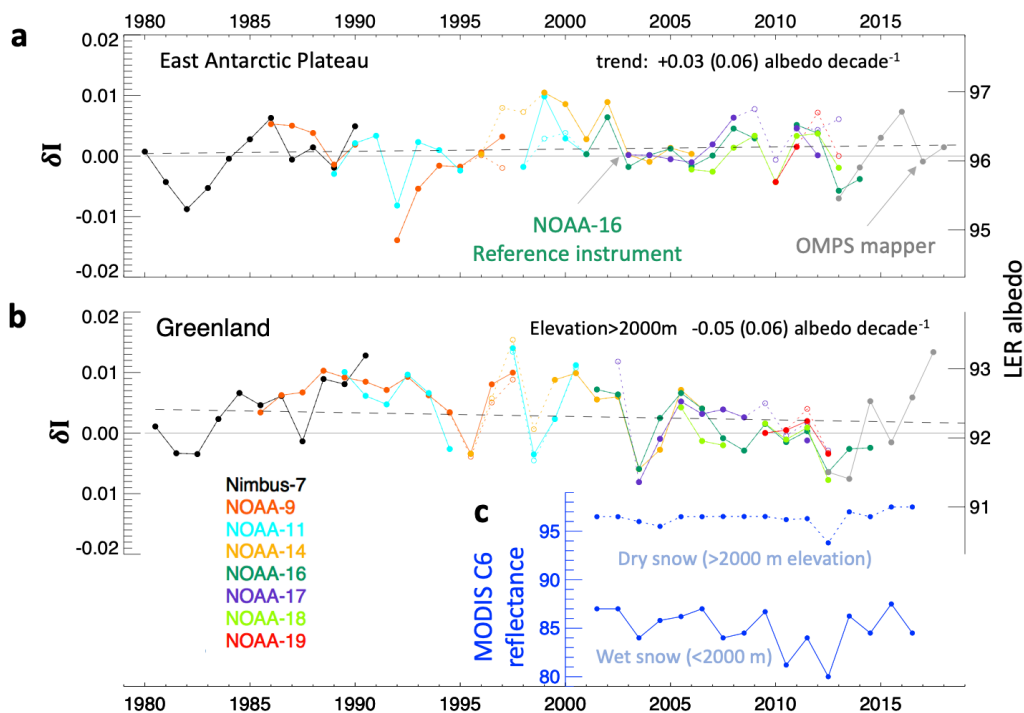
9

Figure 3. δI for all FOVs observed over the ice sheets plotted against solar zenith angle (θ_0) for specific years. The large circles are averages of δI binned by solar zenith angle. Figure 3a shows the previously calibrated δI on the left and our empirically calibrated δI over Antarctica on the right for 2006. Figure 3b is same but over Greenland for 2006. Figure 3c shows our empirically calibrated values over Antarctica in 1992 and Greenland in 1995.



1

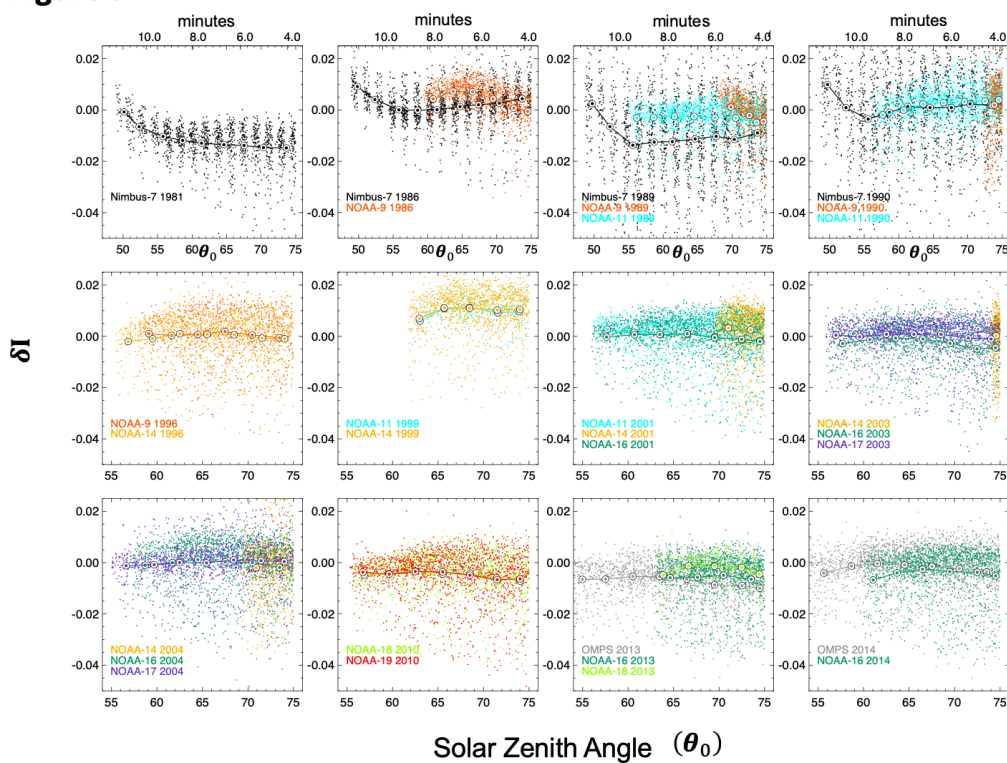
Figure 4



2
 3 Figure 4. Inter-annual variability of our δI for the SBUV instruments (colored) and the
 4 OMPS Mapper (grey) over Antarctica (a) and interior locations over Greenland with ice
 5 surface elevations above 2000 meters (b). The right-hand axis shows the corresponding
 6 change in LER. Annual means plotted with solid circles only include observations with
 7 correct grating drive positions; open circles also include those with grating drive errors
 8 that have been corrected (see text). The lowest panel (Figure 4c) shows MODIS Collection 6
 9 reflectance for Band 3 (459nm) at elevations above 2000 meters (dry snow conditions
 10 dashed trace) and below 2000 meters (wet snow conditions solid trace).
 11



Figure 5

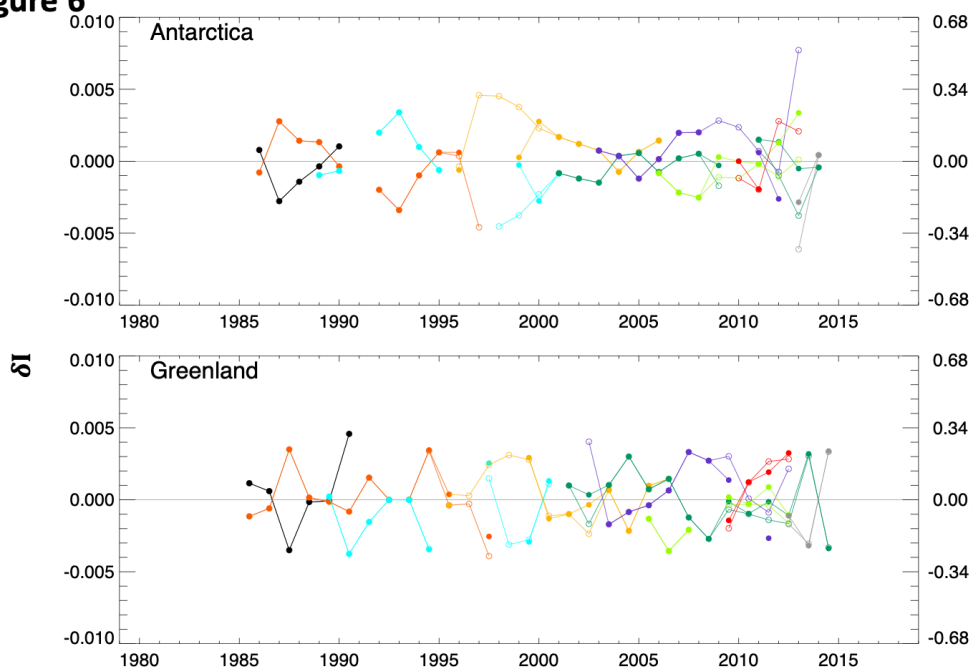


1
2
3
4
5
6
7
8

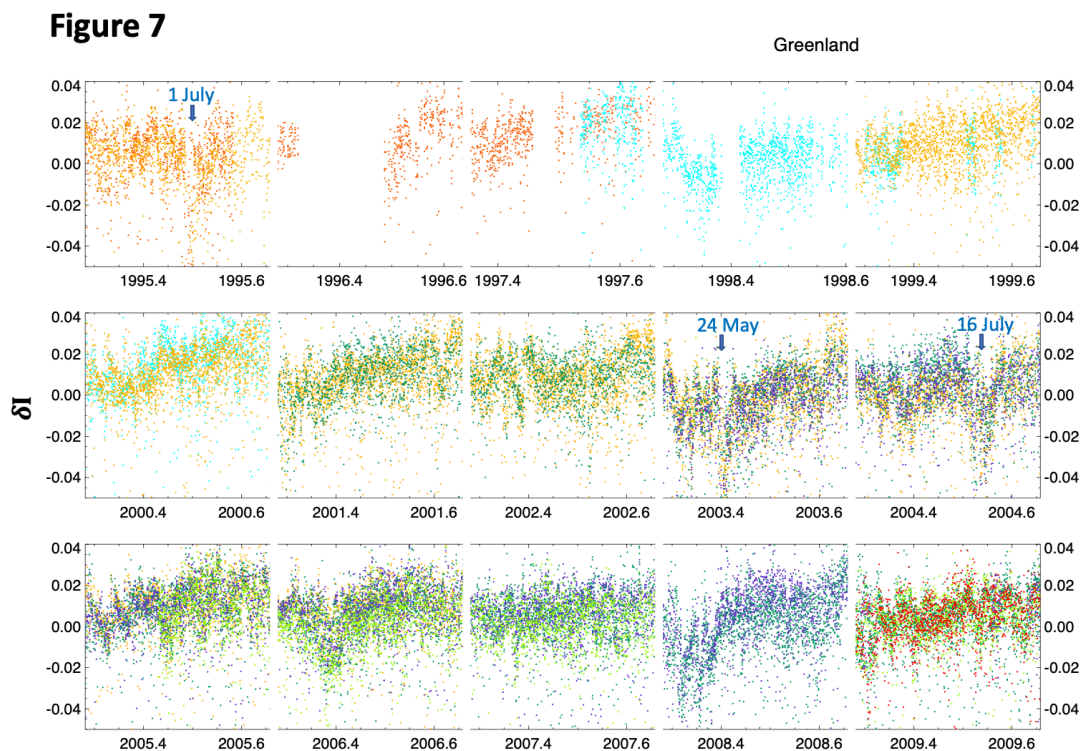
Figure 5. Empirically calibrated for all FOVs observed over Antarctica plotted against solar zenith angle (θ_0) for selected years. The top four panels show the suppression of δI during the first 7-10 minutes after Nimbus-7 sees its first light at the start of a new orbit. At first light, time=0 and $\theta_0=90^\circ$. The time after first light (minutes) is shown at top of first four panels.



Figure 6



- 1
- 2 Figure 6. same as Figure 4 except that merged-satellite average is removed.
- 3



1
2 Figure 7. Time series of empirically calibrated δI for all FOVs observed over Greenland for
3 selected years. Blue arrows indicate estimated dates when CO from boreal forest fires
4 reach Greenland (see text). Color scheme is same as other figures.